Chalcogenide Letters Vol. 22, No. 11, November 2025, p. 959 - 964

Thin-Film Solar Cell Based on $Sb_2(S_x,Se_{1-x})_3$ Solid Solution Films

T. M. Razykov[1], K. M. Kuchkarov[1], R. T. Yuldoshov[1], M. P. Pirimmatov[1], R. R. Khurramov[1], D. Z. Isakov[1], M. A. Makhmudov[1], A. Matmuratov[1], J. G. Bekmirzoyev[1] and A. N. Olimov[2]

[1]Physical-Technical Institute, Uzbekistan Academy of Sciences, Chingiz Aytmatov Street 2B, Tashkent, 100084, Uzbekistan
[2]Institute of Ion-Plasma and Laser Technologies, Uzbekistan Academy of Sciences, 33, Durmon Yuli St., Tashkent, 100125, Uzbekistan
*Corresponding Author: T. M. Razykov. Email: k.kuchkarov@mail.ru

Received: 14 August 2025; Accepted: 11 November 2025

ABSTRACT: This work presents the results of investigating the photovoltaic characteristics of $Sb_2(S_xSe_{1-x})_3$ thin film solar cells manufactured on glass substrates with molybdenum coating using the chemical molecular beam deposition method. Illuminated IV and spectral response measurements on $Sb_2(S_xSe_{1-x})_3$ alloy films show that the device with S/(S + Se) = 0.6 delivers the best performance, reaching 6.47% power-conversion efficiency with V_{OC} = 523 mV, J_{SC} = 27.2 mA cm^{-2}, and a fill factor of 46.71%.

KEYWORDS: Chemical molecular beam deposition; $Sb_2(S_xSe_{1-x})_3$; CdS; ZnO; thin-film solar cell; light IV characteristics; spectral characteristics

1 Introduction

In recent years, several techniques have been developed for obtaining $Sb_2(S_xSe_{1-x})_3$ thin films. The introduction of new structures and the investigation of their physical properties have led to increased solar cell efficiency. To date, efficiencies of 5.6% [1], 5.79% [2], 7.3% [3], and 10.5% [4] have been achieved for solar cells based on novel structures such as FTO/TiO_2/$Sb_2(S_{0.32},Se_{0.68})_3$/Au; ITO/CdS/$Sb_2(S_{0.2}Se_{0.8})_3$/Au; and FTO/CdS/$Sb_2(S,Se)_3$/Spiro/Au, by adjusting selenium and sulfur content in the absorber layer through control of the S/Se ratio. Furthermore, solar cell efficiency is closely related to the fabrication method of the absorber layer. Currently, various methods are used to fabricate the absorber layer in solar cells, including low-vacuum, high-vacuum, and chemical approaches. Non-vacuum technologies have certain advantages. Huanxin Ju and co-authors fabricated solar cells with an efficiency of 5.8% using the direct solution deposition method [5] on the superstrate configuration of FTO/TiO_2/$Sb_{1.9}S_{2.2}Se_{0.9}$/Au. In 2018, a group led by Tao Chen achieved 6.08% efficiency using the hydrothermal deposition method [6]. By 2020, after optimizing the selenization of the absorber layer, they reached an efficiency of 10.5% [4]. Additionally, vacuum-based deposition of the absorber layer with structures such as FTO/TiO_2/$Sb_2(S_{0.32}Se_{0.68})_3$/Au and ITO/CdS/$Sb_2(S_{0.2}Se_{0.8})_3$/Au has yielded promising results. Using the co-evaporation method and the FTO/CdS/ $Sb_2(S_xSe_{1-x})_3$/Ag structure, a solar cell with 5.6% efficiency was also obtained [1]. Furthermore, the group led by Jiang Tang demonstrated the possibility of obtaining polycrystalline $Sb_2(S_xSe_{1-x})_3$ films from Sb_2Se_3 and Sb_2S_3 powders under low vacuum conditions, owing to their low melting temperatures and high vapor pressures. Based on this, they proposed a rapid heating process and a low-vacuum method (8 mTorr), which resulted in a solar cell efficiency of 5.79% [2]. In 2021, a group led by Xiaobo Hu achieved 7.3% efficiency using a vapor deposition method [3]. As of today, the highest reported efficiency of 10.7% for solar cells based on $Sb_2(S_xSe_{1-x})_3$ absorber layers has been obtained using the hydrothermal deposition method [7].

A detailed analysis indicates that the short-circuit current density (J_{SC}) of the solar cells based on $Sb_2(S,Se)_3$ is close to the theoretical Shockley–Queisser limit [8]. However, the the fill factor (FF) and open-circuit voltage (V_{oc}) remain significantly below these theoretical values. The origin of losses in Voc and FF has not yet been fully elucidated and is still under investigation, as noted by several authors [9,10]. Even so, the progress achieved to date has catalyzed rapid advances in Sb_2X_3-based solar cells in recent

https://doi.org/10.15251/CL.2025.2211.959

years. Optimization of the deposition process during hydrothermal synthesis has enabled the formation of more homogeneous $Sb_2(S,Se)_3$ films with enlarged grain sizes and improved electrical properties, leading to an efficiency of 10.5% [4]. Encouraged by these outcomes, Zhao et al. applied a post-processing method that modulate the atomic ratio of S/Se in the $Sb_2(S_xSe_{1-x})_3$ fim and adjusting band alignment, which is beneficial for carrier transport and delivered a 10.7% record efficiency [7]. Li and colleagues improved the chemical bath deposition (CBD) method using a hydrothermal approach for synthesizing Sb_2S_3 and Sb_2Se_3 films, achieving efficiencies of 8% and 10.57%, respectively [11,12]. These studies demonstrate that the development of new deposition techniques for obtaining high-quality Sb_2X_3 films is one of the key solutions for improving the efficiency of Sb_2X_3-based solar cells.

Each approach listed above entails substantial complexity, notably the need to maintain stringent vacuum, and typically relies on supplemental treatments (such as annealing) and high-purity, specification-controlled chemicals to optimize the absorber layer. The chemical molecular beam deposition (CMBD) route used here circumvents these limitations and enables composition-tunable thin films without post-treatments, simply by adjusting deposition time, substrate/precursor temperatures, and carrier-gas flow [13].

2 Experimental Part

Solar cells based on $Sb_2(S_xSe_{1-x})_3$ solid solution films were fabricated on glass substrates coated with a molybdenum layer. The fabrication process and structure of the thin-film solar cell on glass substrates with molybdenum coating are shown in Figs. 1 and 2.

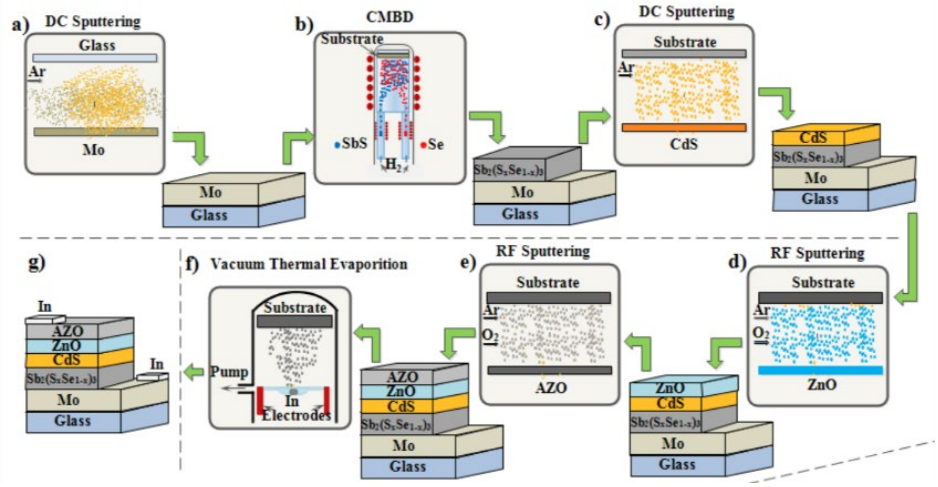

Figure 1: Fabrication process of thin-film solar cells based on $Sb_2(S_xSe_{1-x})_3$. a) Molybdenum coating on glass substrate; b) $Sb_2(S_xSe_{1-x})_3$ thin film deposition; c) preparation of CdS electron-transporting layer; d, e) obtaining ZnO and AZO layers, respectively; f) preparation of the indium electrodes by thermal evaporation; g) the configuration of the obtained solar cell.

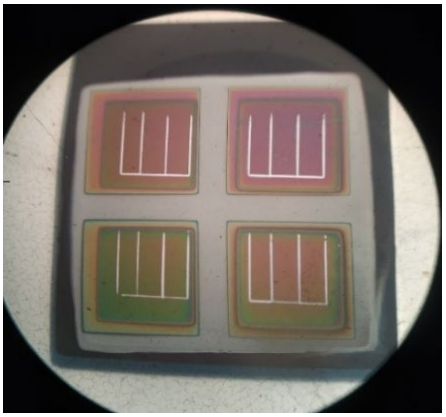

Figure 2: Laboratory-scale solar cell sample based on $Sb_2(S_xSe_{1-x})_3$ solid solution films.

To promote ohmic contact, a 20–30 nm MoSe interlayer was deposited on Mo-coated glass; $Sb_2(S_xSe_{1-x})_3$ was then grown by CMBD at 420°C substrate temperature. The resulting film thickness ranged from approximately 2 to 3 μm, depending on the deposition time. CdS layers were deposited onto the surface of the Mo/MoSe/ $Sb_2(S_xSe_{1-x})_3$ structures via thermal evaporation (thickness 80–100 nm, at a pressure of 10^{-5} mm Hg and substrate temperature of 200°C). To improve the electrical and photovoltaic properties of the Mo/MoSe/ $Sb_2(S_xSe_{1-x})_3$ /CdS heterostructures, thermal treatment was performed in a sealed chamber under pure argon atmosphere.

Thermal treatment was performed in argon (~1 mbar) at 200°C for 20–30 min. To further enhance the photoelectric characteristics, transparent conductive ZnO films (50 nm thick) and Al-doped ZnO (ZnO:Al) films (200–300 nm thick) were deposited on the front contact of the Mo/MoSe/$Sb_2(S_x,Se_{1-x})_3$/CdS heterostructures using magnetron sputtering.

Device metrics J_{SC}, V_{OC}, FF, and η—were extracted from illuminated J–V measurements under 100 mW cm^{-2} irradiance; a solar simulator reproduced the solar spectrum under laboratory conditions.

3 Results and Discussions

Fig. 3 and Table 1 present the I-V measurement results under the illumination of the solar cells for different Se contents, aimed at studying the influence of Se content in the vapor phase on solar cell performance.

Table 1: Post-anneal photovoltaic characteristics of $Sb_2(S_x,Se_{1-x})_3$ thin-film solar cells.

Sample No.	Composition x = [S/(S + Se) in Vapor Phase]	E_g (eV)	Voc (mV)	Jsc (mA/cm^2)	Rsh (Ω)	Rs (Ω)	FF (%)	Efficiency (%)
Ra1	1 (Sb_2S_3)	1.7	545.38	16.4	255.25	47.81	38.18	3.17
Ra3	0.9	1.65	530.61	18.8	222.35	40.72	36.42	3.55
Ra5	0.8	1.5	522.38	27.2	288.31	35.66	38.46	5.31
Ra6	0.7	1.35	523.82	27.2	370.47	18.9	46.71	6.47
Ra4	0.6	1.2	498.07	18.7	365.94	21.22	48.13	4.53
Ra2	0 (Sb_2Se_3)	1.1	383.68	24.8	82.26	24.08	30.55	2.82

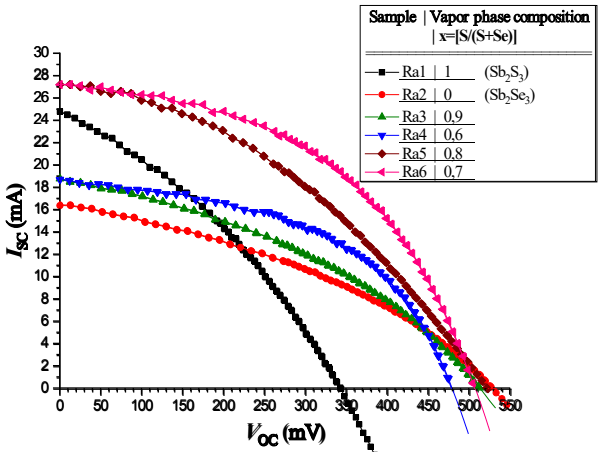

Figure 3: Light J–V characteristics of thin-film photovoltaic devices.

Overall, devices exposed to a Se-richer vapor tended to exhibit superior photovoltaic metrics. The champion cell with S/(S + Se) = 0.6 delivered 6.47% efficiency (V_{OC} = 523 mV, J_{SC} = 27.2 mA cm^{-2}, FF = 46.71%), while most structures showed fill factors around 40%. The V_{OC} and J_{SC} trends versus Se content are summarized in Fig. 3: as expected, V_{OC} decreases progressively with increasing Se due to an upward shift of the Fermi level and the valence-band maximum (VBM), whereas J_{SC} first increases and then declines at x = 0.9. This rise is attributed to band-gap narrowing (E_g reduction) and enhanced crystallinity. The subsequent drop likely results from a modest deterioration in film quality due to a larger S/Se compositional disparity, which impedes charge-carrier transport through the film.

The evolution of series (R_s) and shunt (R_{sh}) resistances is likewise informative for transport analysis. Owing to the higher electrical conductivity of Sb_2Se_3 versus Sb_2S_3, Se-rich devices exhibit lower R_s, yielding improved electrical characteristics and higher J_{SC}. With increasing Se content, R_{sh} also decreases progressively (Table 1), indicating more parallel leakage paths and greater bypass current, consistent with the observed reduction in V_{OC}.

As shown in Table 1, the highest value for η is observed at a composition ratio of approximately x ≈ 0.7. This is attributed to the increased band gap width of the $Sb_2(S_xSe_{1-x})_3$ solid solution films.

Fig. 4 presents the external QE spectra of as obtained solar cells for six compositions (x = 0, 0.6, 0.7, 0.8, 0.9, 1), where the vapor-phase S/(S + Se) ratio was controlled during growth. To ensure accuracy, all devices were measured on the same day under identical conditions with an illuminated spot smaller than the device area. Consistent with the J–V data, the x = 0.6 cell shows the highest QE, peaking near 90% in the 450–650 nm range. The short-wavelength roll-off arises from parasitic absorption in the CdS buffer, while the long-wavelength decline reflects incomplete absorption of IR photons and limited collection of carriers generated far from the depletion region. As x increases, $Sb_2(S_xSe_{1-x})_3$ cells exhibit a stronger response beyond 650 nm, primarily due to band-gap narrowing.

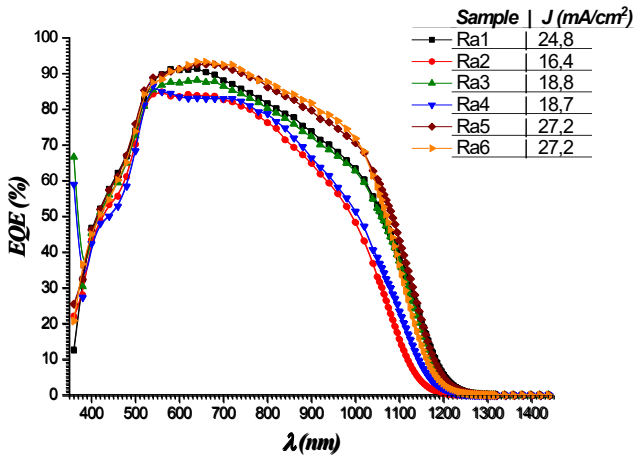

Figure 4: Quantum efficiency of $Sb_2(S_xSe_{1-x})_3$-based thin-film solar cells.

4 Conclusion

For the first time, $Sb_2(S_{1-x}Se_x)_3$ solar cells with absorber layer of the varying composition were fabricated using the chemical molecular beam deposition method. The results of light IV measurements and spectral characterization of heterostructure solar cells with an $Sb_2(S_xSe_{1-x})_3$ absorber layer showed that thermal treatment improved their photovoltaic properties. The measured photovoltaic parameters were: V_{OC} = 383–545 mV; J_{SC} = 16.4–27.2 mA/cm^2; FF = 30.55–48.13%; and efficiency η = 2.82–6.47%. Thermal treatment revealed the optimal annealing conditions for improved photovoltaic performance: temperature T_{ann} = 300°C and duration t_{ann} = 30 min.

Acknowledgement: This work was supported by the Basic Research Program of the Academy of Sciences of the Republic of Uzbekistan and by the Ministry of Innovative Development of the Republic of Uzbekistan. (Grant No. FL-8824063282).

Funding Statement: The authors received no specific funding for this study.

Author Contributions: The authors confirm contribution to the paper as follows: study conception and design: Takhirdjon Razykov, Kudrat Kuchkarov, Mirzavqiy Makhmudov; data collection: Ruhiddin Yuldoshov; analysis and interpretation of results: Kudrat Kuchkarov, Abdurauf Olimov, Ramozan Khurramov, Muhammad Pirimmatov; draft manuscript preparation: Kudrat Kuchkarov, Javokhir Bekmirzoyev, Diyorbek Isakov, Abdurauf Olimov and Aydos Matmuratov. All authors reviewed the results and approved the final version of the manuscript.

Availability of Data and Materials: Data available on request from the authors.

Conflicts of Interest: The authors declare no conflicts of interest to report regarding the present study.

References

1. Zhou Y, Wang L, Chen S, Qin S, Liu X, Chen J, et al. Thin-film Sb_2Se_3 photovoltaics with oriented one-dimensional ribbons and benign grain boundaries. Nat Photon. 2015;9:409–15. https://doi.org/10.1038/nphoton.2015.78.
2. Yang B, Qin S, Xue D, Chen C, He Y, Niu D, et al. *In situ* sulfurization to generate $Sb_2(Se_{1-x}S_x)_3$ alloyed films and their application for photovoltaics. Prog Photovolt Res Appl. 2016;25:113–22. https://doi.org/10.1002/pip.2819.
3. Hu X, Tao J, Wang R, Wang Y, Pan Y, Weng G, et al. Fabricating over 7%-efficient $Sb_2(S,Se)_3$ thin-film solar cells by vapor transport deposition using Sb_2Se_3 and Sb_2S_3 mixed powders as the evaporation source. J Power Sources. 2021;493:229737; https://doi.org/10.1016/.jpowsour.2021.229737.
4. Wang X, Tang R, Jiang C, Lian W, Ju H, Jiang G, et al. Manipulating the electrical properties of $Sb_2(S,Se)_3$ film for high-efficiency solar cell. Adv Energy Mater. 2020; 10:2002341.

https://doi.org/10.1002/aenm.202002341.
5. Wu C, Zhang L, Ding H, Ju H, Jin X, Wang X, et al. Direct solution deposition of device quality Sb2S3-xSex films for high efficiency solar cells. Sol Energy Mater Sol Cells. 2018; 183:52–8. https://doi.org/10.1016/j.solmat.2018.04.009.
6. Wang W, Wang X, Chen G, Yao L, Huang X, Chen T, et al. Over 6% certified $Sb_2(S,Se)_3$ solar cells fabricated via *in situ* hydrothermal growth and postselenization. Adv Electron Mater. 2018;5:201800683. https://doi.org/10.1002/aelm.201800683.
7. Li K, Tang R, Zhu C, Chen T. Critical review on crystal orientation engineering of antimony chalcogenide thin film for solar cell applications. Adv Sci. 2023;11:e2304963. https://doi.org/10.1002/advs.202304963.
8. Rühle S. Tabulated values of the shockley–queisser limit for single junction solar cells. Sol Energy. 2016;130:139–47. https://doi.org/10.1016/j.solener.2016.02.015.
9. Chen C, Tang J. Open-circuit voltage loss of antimony chalcogenide solar cells: status, origin, and possible solutions. ACS Energy Lett. 2020;5:2294–304. https://doi.org/10.1021/acsenergylett.0c00940.
10. Dong J, Liu Y, Wang Z, Zhang Y. Boosting V_{OC} of antimony chalcogenide solar cells: a review on interfaces and defects. Nano Sel. 2021;2:1818–48. https://doi.org/10.1002/nano.202000288.
11. Wang S, Zhao Y, Che B, Li C, Chen X, Tang R, et al. A novel multi-sulfur source collaborative chemical bath deposition technology enables 8%-efficiency Sb_2S_3 planar solar cells. Adv Mater. 2022;34:e2206242. https://doi.org/10.1002/adma.202206242.
12. Zhao Y, Wang S, Li C, Che B, Chen X, Chen H, et al. Regulating deposition kinetics *via* a novel additive-assisted chemical bath deposition technology enables fabrication of 10.57%-efficiency Sb_2Se_3 solar cells. Energy Environ Sci. 2022;15:5118–28. https://doi.org/10.1039/d2ee02261c.
13. Razykov T. Chemical molecular beam deposition of II–VI binary and ternary compound films in a gas flow. Appl Surf Sci. 1991;48–49:89–92. https://doi.org/10.1016/0169-4332(91)90311-7.